Supplementary Information (SI)

A major combustion aerosol event had a negligible impact on the atmospheric ice-nucleating particle population

M. P. Adams[1], M. D. Tarn[1,2], A. Sánchez-Marroquín[1], G. C. E. Porter[1,2], D. O'Sullivan[1,*], A. D. Harrison[1], Z. Cui[1], J. Vergara-Temprado[1,+], F. Carotenuto[3,4,^], M. A. Holden[1,2,5,~], M. Daily[1], T. F. Whale[1,5,>], S. N. F. Sikora[1], I. T. Burke[6], J.-u. Shim[2], J. B. McQuaid[1] and B. J. Murray[1]

1 – Institute of Climate and Atmospheric Science, School of Earth and Environment, University of Leeds, Woodhouse Lane, LS2 9JT, UK
2 –School of Physics and Astronomy, University of Leeds, Woodhouse Lane, LS2 9JT, UK
3 – University of Innsbruck, 6020, Austria
4 – CNR Institute of BioMeteorology, Florence, 50019, Italy
5 – School of Chemistry, University of Leeds, Woodhouse Lane, LS2 9JT, UK
6 – Earth Science Institute, School of Earth and Environment, University of Leeds, Woodhouse Lane, LS2 9JT, UK

* Now at The Stars Group, Wellington place, Leeds, West Yorkshire, UK
+ Now at Institute for Atmospheric and Climate Science, ETH Zürich, Zurich, Switzerland
^ Now at CNR Institute of BioEconomy, Florence, 50019, Italy
~ Now at School of Physical Sciences and Computing, University of Central Lancashire, Fylde Road, Preston, PR1 2HE, UK
> Now at Department of Chemistry, University of Warwick, Gibbet Hill Road, Coventry, CV4 7AL, UK

Corresponding author: Michael Adams (M.P.Adams@leeds.ac.uk)

Contents

Section 1 - Back-trajectory plots and map of area

Figure S1: A map of the a) immediate area around the sampling site b) the wider Leeds area. The light blue line indicates the 0.5 km area surrounding sampling site that is University campus, with the dark blue line showing the 10 km surrounding suburban area.

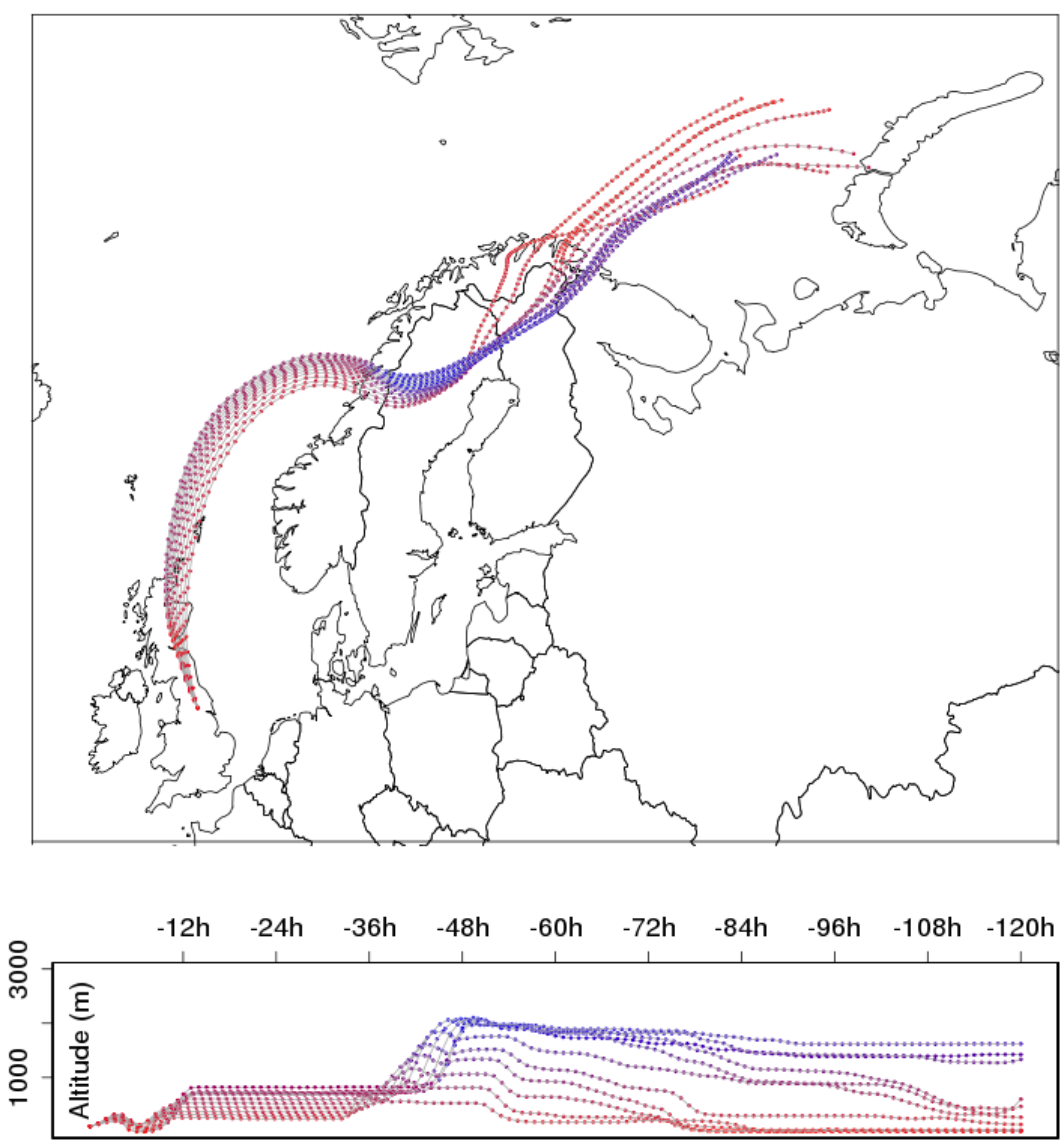

Figure S2: Backward trajectories of air masses during the sampling period on 05/11/2016 (DD/MM/YYY). The back trajectories are shown hourly, up to 120 h prior to the collection of a sample onto a filter. The colour scale shows the altitude of the air masses throughout the back trajectory, with red indicating a lower altitude and blue indicating a higher altitude. The back trajectories were generated using the NOAA HYSPLIT model (Stein et al., 2015).

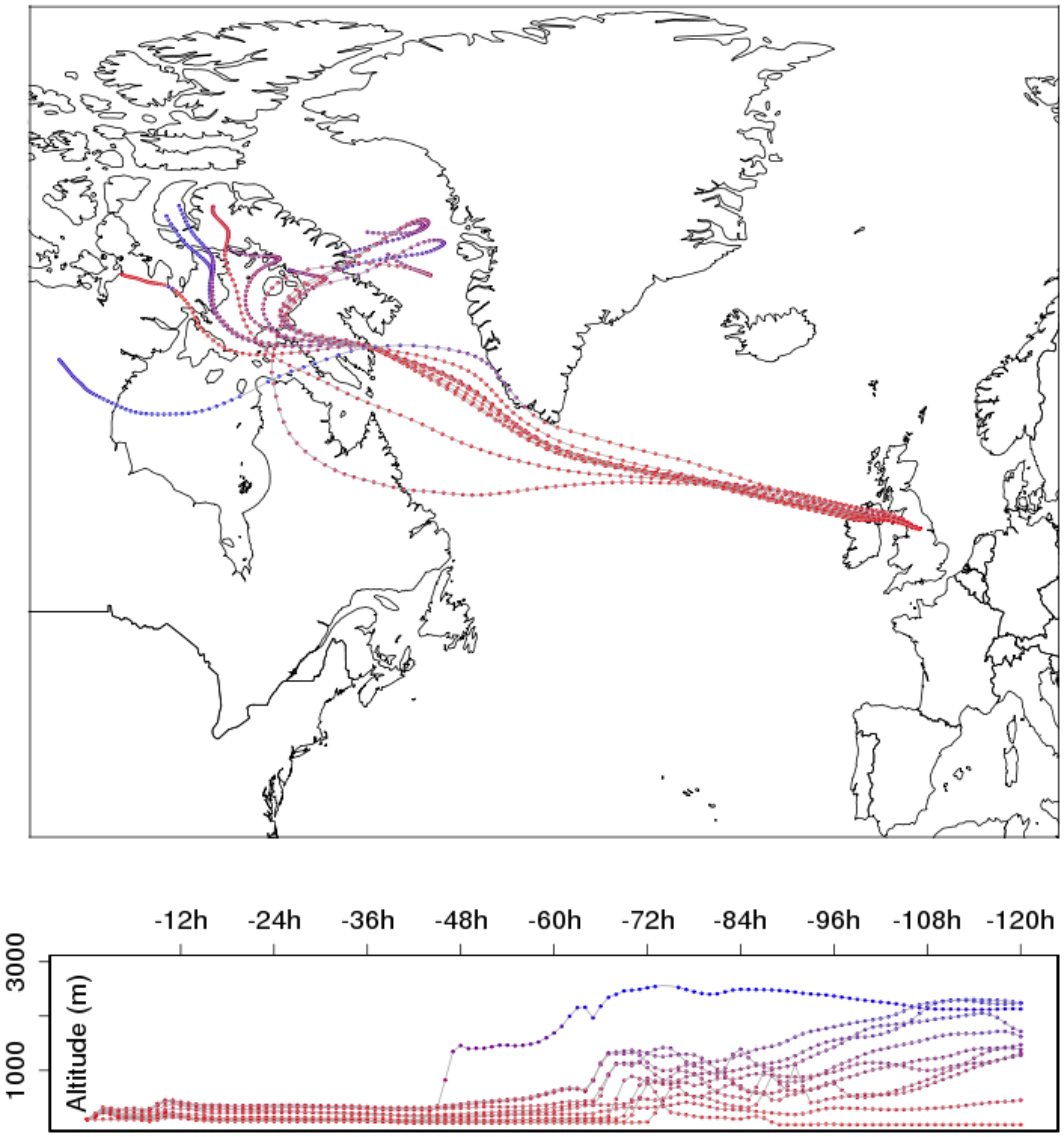

Figure S3: Backward trajectories of air masses during the sampling period 04/11/2017 (DD/MM/YYYY). The back trajectories are shown hourly corresponding approximately to the time of each filter sample. The colour scale shows the altitude of the air masses throughout the back trajectory, with red indicating a lower altitude and blue indicating a higher altitude. The back trajectories were generated using the NOAA HYSPLIT model (Stein et al., 2015).

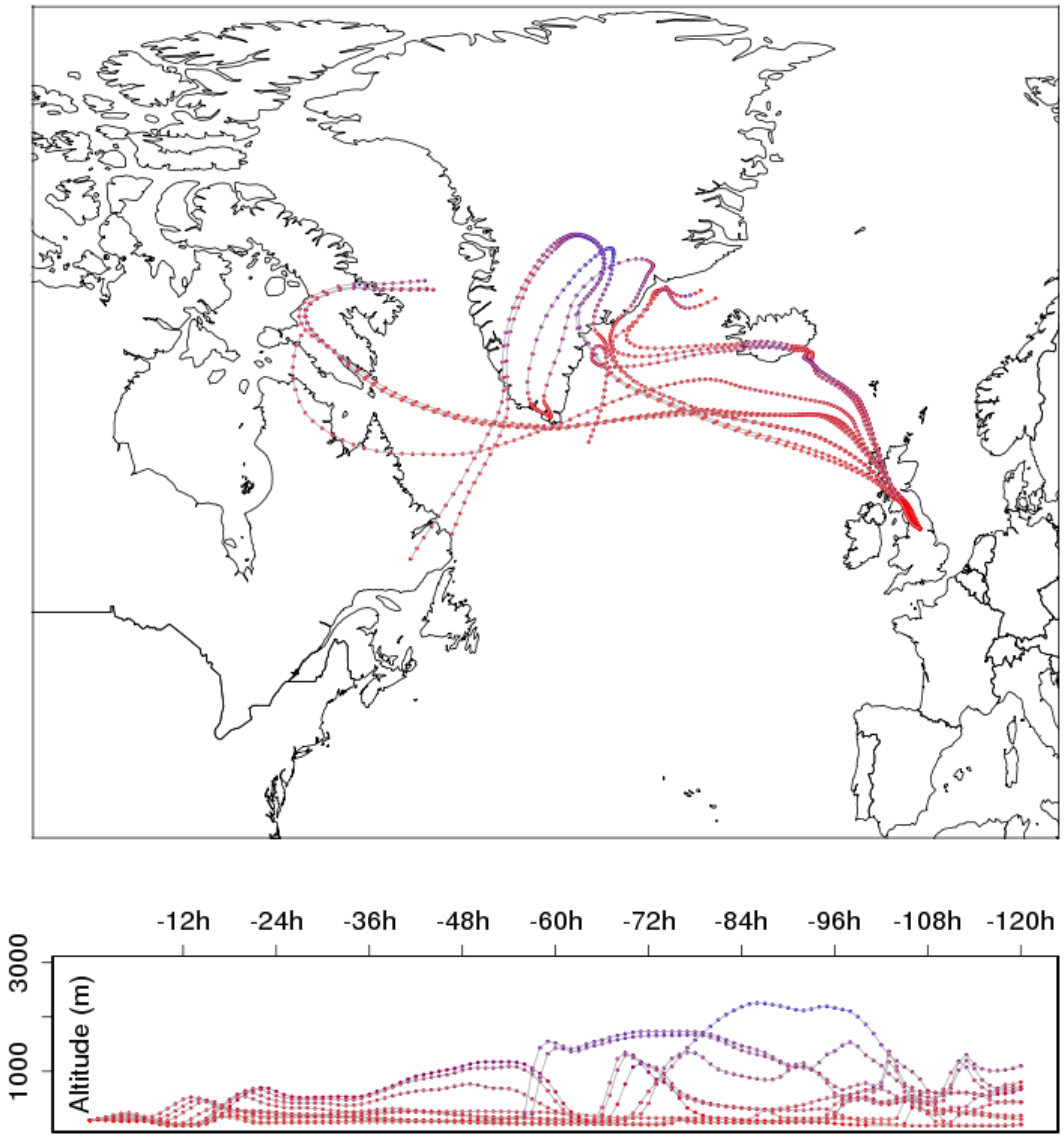

Figure S4: Backward trajectories of air masses during the sampling period 05/11/2017 (DD/MM/YYYY). The back trajectories are shown hourly corresponding approximately to the time of each filter sample. The colour scale shows the altitude of the air masses throughout the back trajectory, with red indicating a lower altitude and blue indicating a higher altitude. The back trajectories were generated using the NOAA HYSPLIT model (Stein et al., 2015).

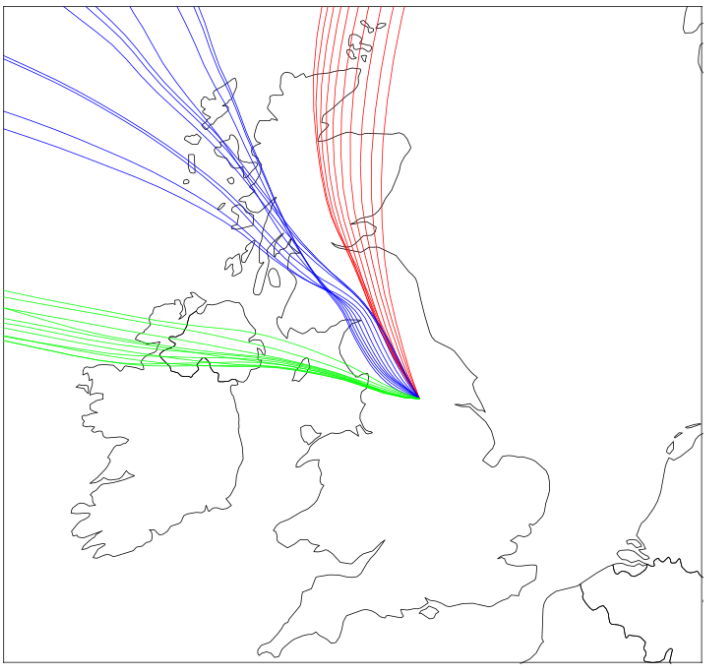

Figure S5: HYSPLIT back trajectories for all three days, zoomed in on the U.K. Red indicates 05/11/2016, green 04/11/2017, blue 05/11/2017.

Section 2 - Fraction frozen curves

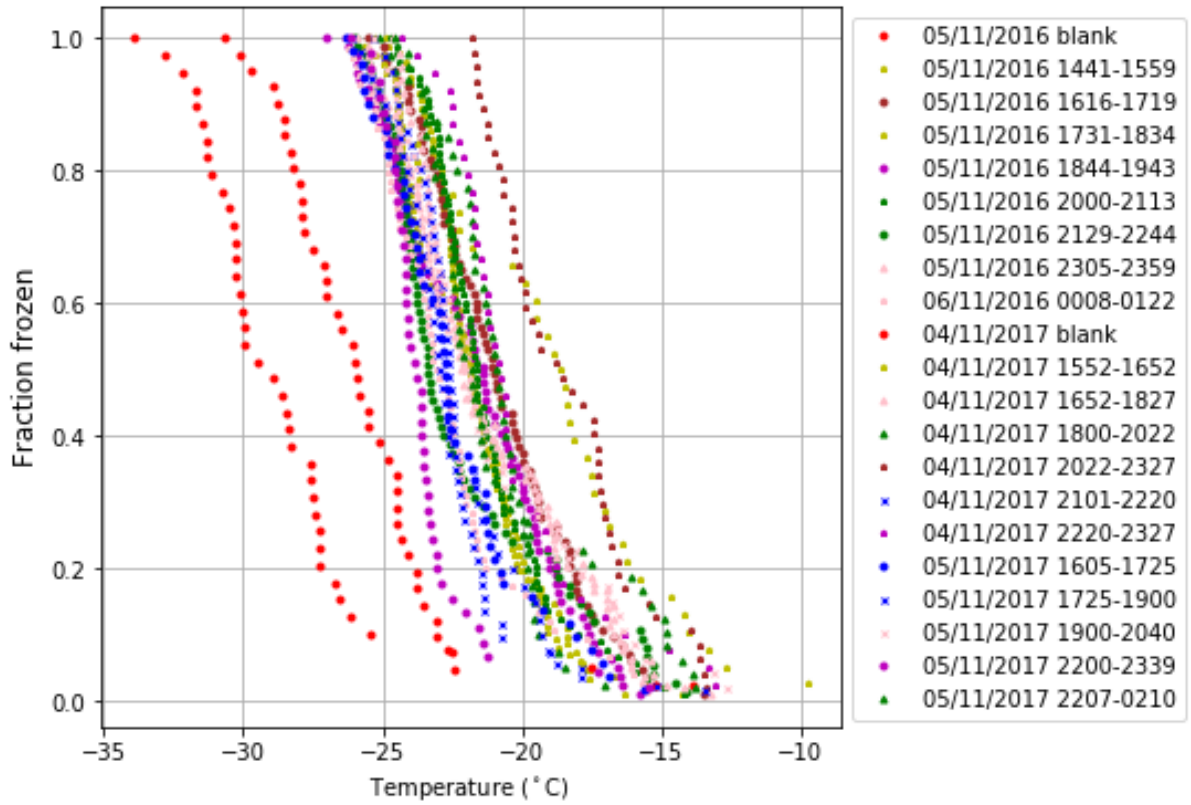

Figure S6: Fraction frozen curves for each sample collected and analysed via the microlitre Nucleation by Immersed Particle Instrument (μL-NIPI) technique during the Bonfire Night festivals over two years. A handling blank was also run each year prior to sampling.

Section 3 – Sampling details for filter-based aerosol collection

Table S1: Sampling times and volumes of air sampled (at 16.7 L min^{-1}) for each filter collected for ice-nucleating particle (INP) analysis during the Bonfire Night festival.

Filter no.	Start time	Midpoint of sampling	End time	Sampling duration (min)	Volume of air sampled (L)
1	05/11/2016 14:41	05/11/2016 15:20	05/11/2016 15:59	78	1300
2	05/11/2016 16:16	05/11/2016 16:48	05/11/2016 17:19	63	1050
3	05/11/2016 17:31	05/11/2016 18:03	05/11/2016 18:34	63	1050
4	05/11/2016 18:44	05/11/2016 19:14	05/11/2016 19:43	59	983
5	05/11/2016 20:00	05/11/2016 20:37	05/11/2016 21:13	73	1216
6	05/11/2016 21:29	05/11/2016 22:07	05/11/2016 22:44	75	1250
7	05/11/2016 23:05	05/11/2016 23:32	05/11/2016 23:59	54	900
8	06/11/2016 00:08	06/11/2016 00:45	06/11/2016 01:22	74	1233
9	04/11/2017 15:52	04/11/2017 16:22	04/11/2017 16:52	60	1000
10	04/11/2017 16:52	04/11/2017 17:40	04/11/2017 18:27	95	1583
11	04/11/2017 18:00	04/11/2017 19:11	04/11/2017 20:22	142	2367
12	04/11/2017 20:22	04/11/2017 21:55	04/11/2017 23:27	185	3083
13	04/11/2017 21:01	04/11/2017 21:41	04/11/2017 22:20	79	1316
14	04/11/2017 22:20	04/11/2017 22:54	04/11/2017 23:27	67	1116
15	05/11/2017 16:05	05/11/2017 16:45	05/11/2017 17:25	80	1333
16	05/11/2017 17:25	05/11/2017 18:13	05/11/2017 19:00	95	1583
17	05/11/2017 19:00	05/11/2017 19:50	05/11/2017 20:40	100	1667
18	05/11/2017 22:00	05/11/2017 22:50	05/11/2017 23:39	99	1650
19	05/11/2017 22:07	06/11/2017 00:09	06/11/2017 02:10	243	4050

Section 4 – Mean and standard deviations of [INP]

Table S2: Mean INP concentrations at selected temperatures for pre-event measurements (defined as measurements taken prior to 18:00) and during event measurements (post 18:00). Also included are standard deviations for all event measurements.

05/11/2016			
Temperature (°C)	Pre-event INP (INP L^{-1})	Event mean INP (INP L^{-1})	Event standard deviation (INP L^{-1})
-17.00	0.34	0.40	0.21
-18.00	0.52	0.62	0.31
-19.00	0.93	0.98	0.46
-20.00	1.53	1.40	0.61
-21.00	2.51	1.92	0.81
-22.00	3.89	3.06	1.25
-23.00	6.86	4.39	1.73
04/11/2017			
Temperature (°C)	Pre-event INP (INP L^{-1})	Event mean INP (INP L^{-1})	Event standard deviation (INP L^{-1})
-17.00	1.71	0.39	0.25
-18.00	2.51	0.57	0.39
-19.00	4.01	0.76	0.49
-20.00	4.98	1.21	0.48
-21.00	5.35	2.11	1.02
-22.00	5.75	3.45	2.51
-23.00	7.19	5.94	4.94
05/11/2017			
Temperature (°C)	Pre-event INP (INP L^{-1})	Event mean INP (INP L^{-1})	Event standard deviation (INP L^{-1})
-17	0.23	0.28	0.21
-18	0.39	0.31	0.25
-19	0.55	0.41	0.34
-20	0.64	0.50	0.40
-21	0.91	0.60	0.47
-22	1.74	1.09	0.70
-23	3.32	2.26	1.22

Section 5 - Description of SEM-EDS category classification and filter loading details

The scanning electron microscopy with energy-dispersive X-ray spectroscopy (SEM-EDS) classification of particles into different categories was achieved using the same methodology as described in Sanchez-Marroquin et al., (2019), with some slight changes: 'Na rich' and 'S rich' particles have been combined into one category, along with unclassified particles (labelled as 'Others'). As described in the main text, particles in the categories of 'Si only', 'Si rich', 'Al-Si rich' ad 'Ca rich' have been considered as being mineral dust or ash.

The aerosol loading on the filters before and after the sampling events are shown in Figure S7.

Figure S7: Filters before (a) and after sampling (b). The dark colour of the filter after ~1 hour sampling during the combustion event is clear. Filter sampling in Leeds during normal conditions does not yield dark filters.

Section 6 – Additional number concentration and size distribution data

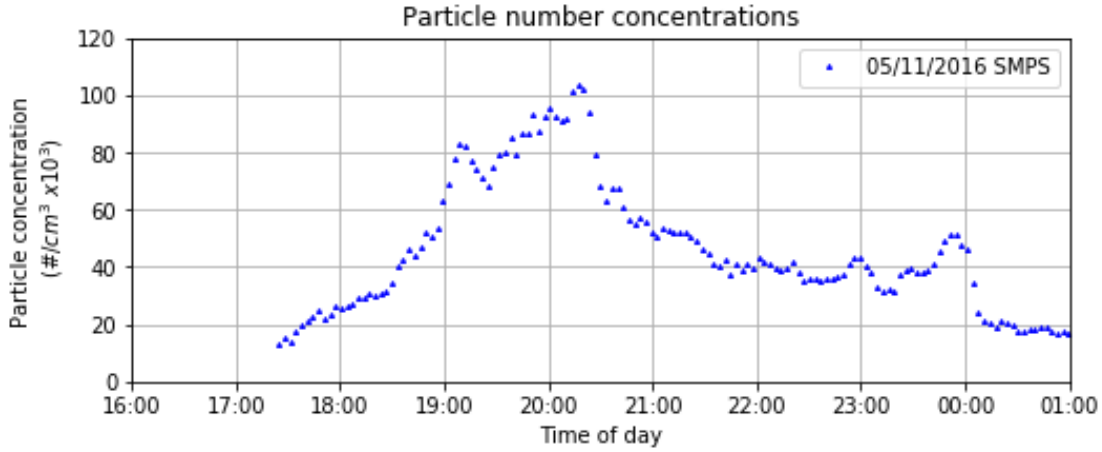

Figure S8: Aerosol number concentrations as measured by the scanning mobility particle sizer (SMPS) on 05/11/2016 (17.5 - 552.3 nm particle diameter range).

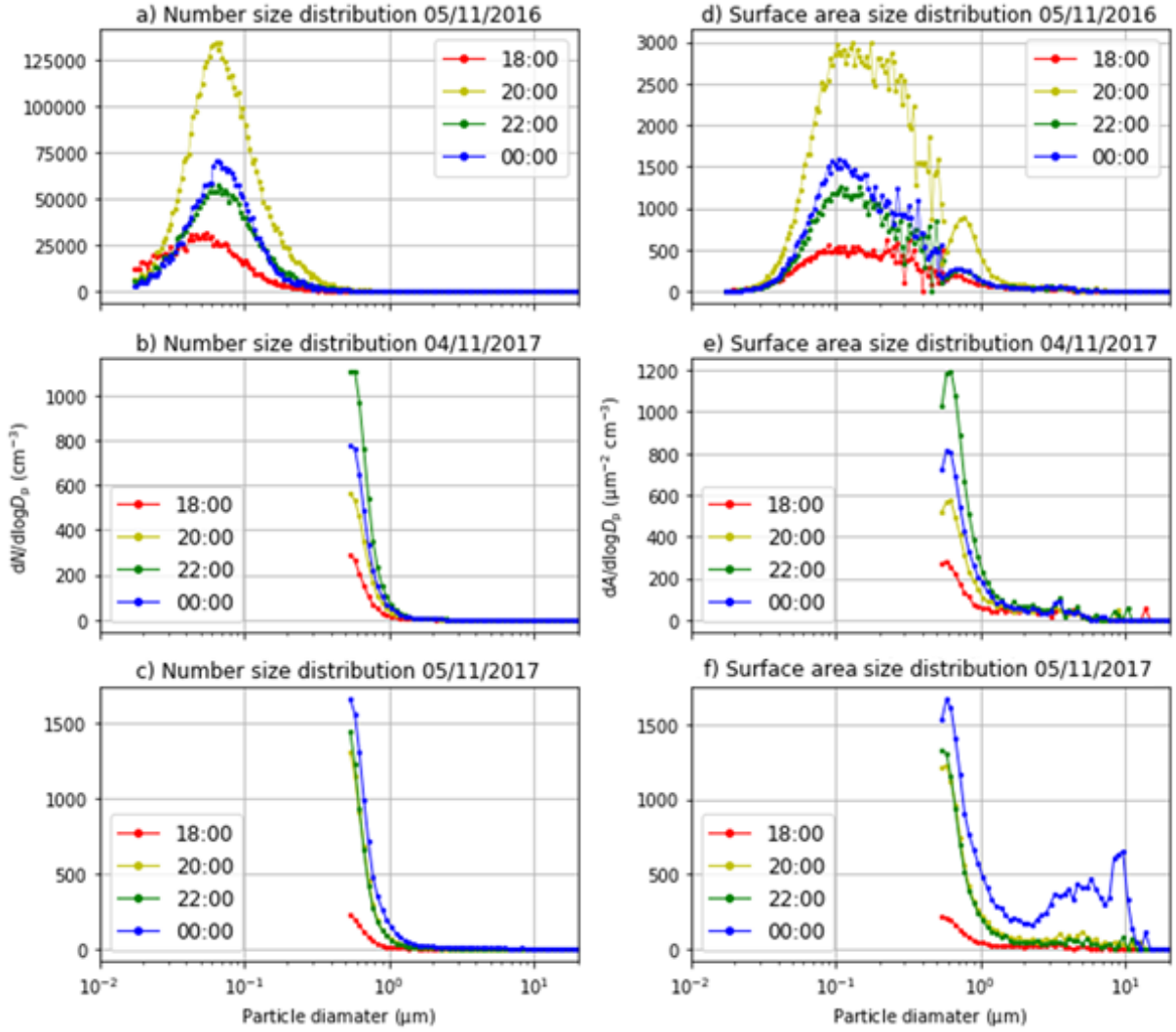

Figure S9: All available particle size distribution data from each sampling event. The SMPS was only available in 2016, and thus panels b, c, e, f have size distributions only above 0.5 microns. The distributions are not corrected to volume equivalent diameter.

Section 7 - PM_{10} data for Leeds city centre

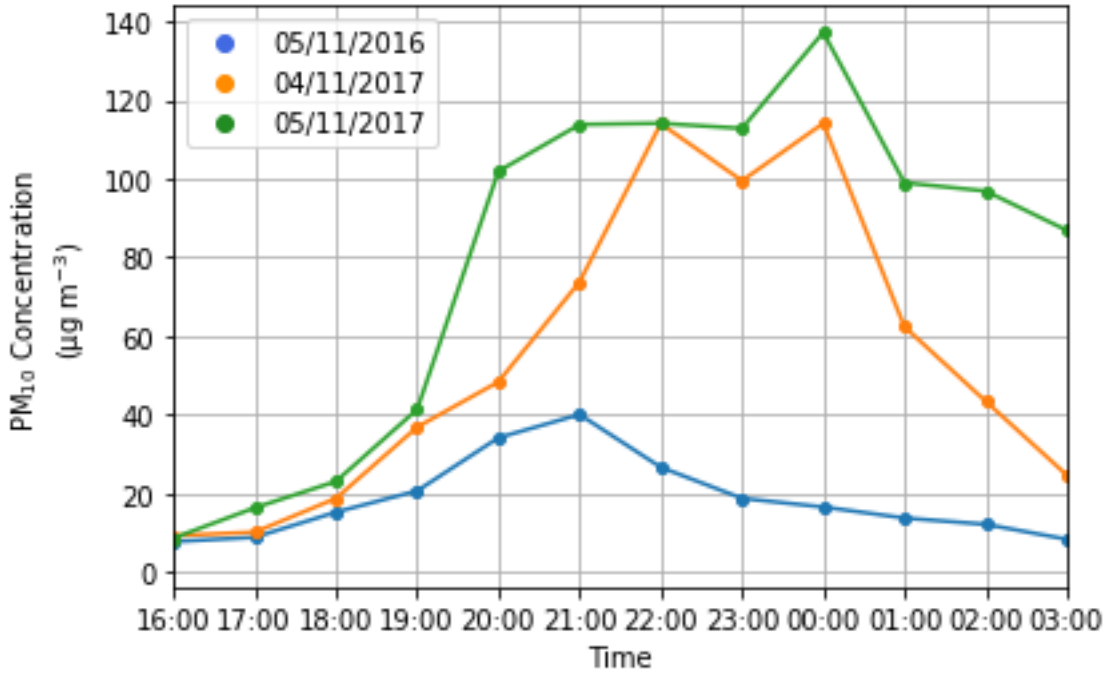

Figure S10: Concentration of particulate matter of 10 µm in diameter or below (PM_{10}) during the evenings over which aerosol sampling took place. The data was collected at a Department of Environment, Food and Rural Affairs (DEFRA) site in Leeds city centre (https://uk-air.defra.gov.uk/networks/site-info?site_id=LEED). This site is approximately 1 km from our sampling site.

Section 8 – Non combustion event INP species

While it was not the focus of this study, it is interesting to question what the INP species were in the atmosphere at this time. O'Sullivan et al. (2018) carried out a detailed study on INP concentrations and species in a location ~19 km from the Bonfire Night sampling site at the same time of year to the measurements made in this study. As such, we refer to the detailed discussion of that paper with regards to the interpretation of what INP species may have contributed to the local INP population. In brief, that study found that background INP concentrations were dominated by mineral dust at T < −18 °C, and above this temperature bio-INPs played an important but highly variable role.

In order to understand the contribution of mineral dust to the INP spectra we report, we used two parameterisations for calculating $[INP]_T$ based on mineral/desert dust surface area, in conjunction with the SEM-EDS mineral dust/ash surface area from section 3.3. We used two different mineral dust parameterisations, one based on the ice-active K-feldspar content of desert dust (H19) and one based on measurements of freshly dispersed desert dust (N12) (Harrison et al., 2019; Niemand et al., 2012). For the H19 parameterisation, a 1 wt. % concentration of K-feldspar has been assumed. The predictions are shown in Figure S11. The shaded area for each parameterisation shows the range of INP concentrations predicted by the surface area concentrations from both the "early" and "peak" filters analysed using SEM-EDS, including uncertainties. The figure shows that both parameterisations capture some of the data below –20 °C, with INP concentrations above –20 °C sometimes being above the ranges predicted by both N12 and H19. The N12 parameterisation predicts a higher INP concentration than H19 above about -20 °C, which is a better fit to the data, however INP measurements in desert dust plumes indicate that N12 produces too high an ice nucleation activity in transported dust, especially above about -20 °C (Price et al., 2018). No heat tests were performed in this study, so it is not possible to distinguish between heat sensitive biological INPs and non-heat sensitive INP like mineral dust. Nevertheless, the results in Figure S11 are consistent with those of O'Sullivan et al. (2018).

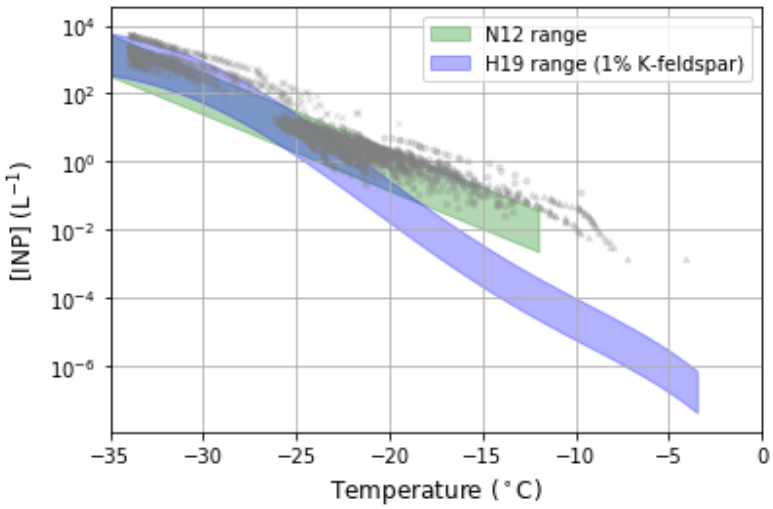

Figure S11: A plot showing $[INP]_T$ values measured during the sampling events, overlaid with [INP] predictions based on the Niemand 2012 (N12) and Harrison 2019 (H19) parametrisation and surface area concentration obtained from SEM-EDS analysis.

References

Harrison, A. D., Lever, K., Sanchez-Marroquin, A., Holden, M. A., Whale, T. F., Tarn, M. D., et al. (2019). The ice-nucleating ability of quartz immersed in water and its atmospheric importance compared to K-feldspar. *Atmospheric Chemistry and Physics*, *19*(17), 11343–11361. https://doi.org/10.5194/acp-19-11343-2019

Niemand, M., Möhler, O., Vogel, B., Vogel, H., Hoose, C., Connolly, P., et al. (2012). A Particle-Surface-Area-Based Parameterization of Immersion Freezing on Desert Dust Particles. *Journal of the Atmospheric Sciences*, *69*(10), 3077–3092. https://doi.org/10.1175/JAS-D-11-0249.1

O'Sullivan, D., Adams, M. P., Tarn, M. D., Harrison, A. D., Vergara-Temprado, J., Porter, G. C. E., et al. (2018). Contributions of biogenic material to the atmospheric ice-nucleating particle population in North Western Europe. *Scientific Reports*, *8*(1), 13821. https://doi.org/10.1038/s41598-018-31981-7

Price, H. C., Baustian, K. J., Mcquaid, J. B., Blyth, A., Bower, K. N., Choularton, T., et al. (2018). Atmospheric Ice-Nucleating Particles in the Dusty Tropical Atlantic. https://doi.org/10.1002/2017JD027560

Sanchez-Marroquin, A., Hedges, D. H. P., Hiscock, M., Parker, S. T., Rosenberg, P. D., Trembath, J., et al. (2019). Characterisation of the filter inlet system on the FAAM BAe-146 research aircraft and its use for size-resolved aerosol composition measurements. *Atmospheric Measurement Techniques*, *12*(11), 5741–5763. https://doi.org/10.5194/amt-12-5741-2019

Stein, A. F., Draxler, R. R., Rolph, G. D., Stunder, B. J. B., Cohen, M. D., & Ngan, F. (2015). Noaa's hysplit atmospheric transport and dispersion modeling system. *Bulletin of the American Meteorological Society*. https://doi.org/10.1175/BAMS-D-14-00110.1